JPEDAV (2005) 26:605-612
DOI: 10.1361/154770305X74421
1547-7037/$19.00 ©ASM International

Thermodynamic Reassessment of the Cu-O Phase Diagram

L. Schramm, G. Behr, W. Löser, and K. Wetzig

(Submitted August 2, 2004; in revised form September 7, 2005)

Parts of the copper-oxygen equilibrium phase diagram were reassessed using the calculation of phase diagram technique (CALPHAD). The model parameters were optimized to yield the best fit between calculated and experimentally determined phase equilibria at elevated oxygen pressures up to 11 MPa. The Cu-O liquid phase is represented by the two-sublattice model for ionic liquids containing copper on the cation sublattice with formal valences of Cu^{+1}, Cu^{+2}, and Cu^{+3}. The presence of Cu^{+3} ions in the liquid phase, corresponding to a formation of Cu_2O_3 species, was the key assumption of this model. Congruent melting of CuO at 1551 K under an oxygen pressure of ~126.8 MPa is predicted, which is considerably below previous theoretical values.

1. Introduction

Copper oxide (CuO, space group *C*2/*c*) has attracted renewed attention because it is the simplest member of a family of compounds, which exhibit physical properties like high-temperature superconductivity, electron correlation effects, and spin dynamics.[1,2]

The copper-oxygen system contains two stable oxides, CuO and Cu_2O, which are both close to their stoichiometric composition. The liquid phase, observed under oxygen pressures <0.1 MPa, corresponds to the composition interval from pure liquid copper to the oxidic melt close to a Cu_2O + CuO eutectic. The metallic character of the melt is separated from the oxidic one by a miscibility gap (Fig. 1). A comprehensive review of experimental data associated with oxygen pressure smaller then 0.1 MPa is given by Hallstedt et al.[3] At higher oxygen pressures the phase equilibria along the CuO-liquidus have been investigated by Roberts and Smyth[4] as well as Kosenko and Emel'chenko.[5] The latter authors revealed the CuO-liquidus as a function of temperature and oxygen pressures up to 11 MPa.

Previous assessments of the copper-oxygen system produced results that agree well with the data for oxygen pressures <0.1 MPa.[3,6-10] At elevated oxygen pressure, a significant deviation between the theoretical and experimental results becomes apparent.

In the present assessment of the Cu-O phase diagram, the authors are using the experimental information on the Cu_2O- and CuO-liquidus based on the experimental work of Roberts and Smyth and Kosenko and Emel'chenko, as well as the Gibbs energy of the CuO phase between 298 and 1364 K evaluated by Glushko and Medvedv (Termicheskie Konstanty Veshchestv) and by JANAF thermochemical tables.[11,12] To fit these data correctly, a two sublattice model for the ionic liquid including the higher valent Cu^{+3} species on the cation sublattice is supposed.

Besides the copper valence of $\upsilon = +1$ and $\upsilon = +2$ in the compounds Cu_2O and CuO and a metastable mixed-valence compound Cu_4O_3 (paramelanokite),[13] a higher copper valences of $\upsilon = +3$ in the compound Cu_2O_3 has also been found.[14] A review of Cu^{+3}-chemistry was given by Scholder and Voelskow.[15] Moreover, Cu-ions with a formal valence $\upsilon > +2$ play a crucial role in complex copper oxides such as high-temperature superconductors like $YBa_2Cu_3O_{6+\delta}$ with ($\delta > 0.5$) or the spin ladder compound $Sr_{14}Cu_{24}O_{41}$ as well as oxidic melts of $Nd_{1.85}Ce_{0.15}CuO_4$ and $Ca_8Sr_6Cu_{24}O_{41}$.[16-18] In the solid compounds the oxidation of Cu in the superconducting $(CuO_2)^{-2}$ sheets (*p*-type superconductors) appears to be controlled by the Cu-O bond length and the oxygen coordination number of the copper atoms. It is commonly accepted that oxidation/reduction of the $(CuO_2)^{-2}$ sheets above/below the formal oxidation state of $\upsilon = -2$ is one of the necessary conditions to induce superconductivity.[19-21]

2. Thermodynamic Modeling

2.1 Gas Phase

In the considered ranges of temperature and pressure, it is assumed that the gas phase of the Cu-O-system consists of gaseous O_2. The molar Gibbs energy of the phase G^{gas} is modeled by the expression:

$$G^{gas} = 2 \cdot G^0_{1/2O_2} + RT \cdot \ln\left(\frac{p}{p_0}\right) \quad \text{(Eq 1)}$$

where the pressure dependence of the Gibbs energy function is taken as ideal. This assumption is acceptable for pressures up to 100 MPa, which was tested using the tabulated van der Waals coefficients published for gaseous O_2 in Ref 22. In Eq 1, the value of $G^0_{1/2O_2}$ is defined as the Gibbs energy

L. Schramm, G. Behr, W. Löser, and **K. Wetzig,** IFW Dresden, Leibniz-Institut für Festkörper- und Werkstoffforschung, P. O. Box 270116, D-01171, Dresden, Germany. Contact e-mail: L.Schramm@ifw-dresden.de.

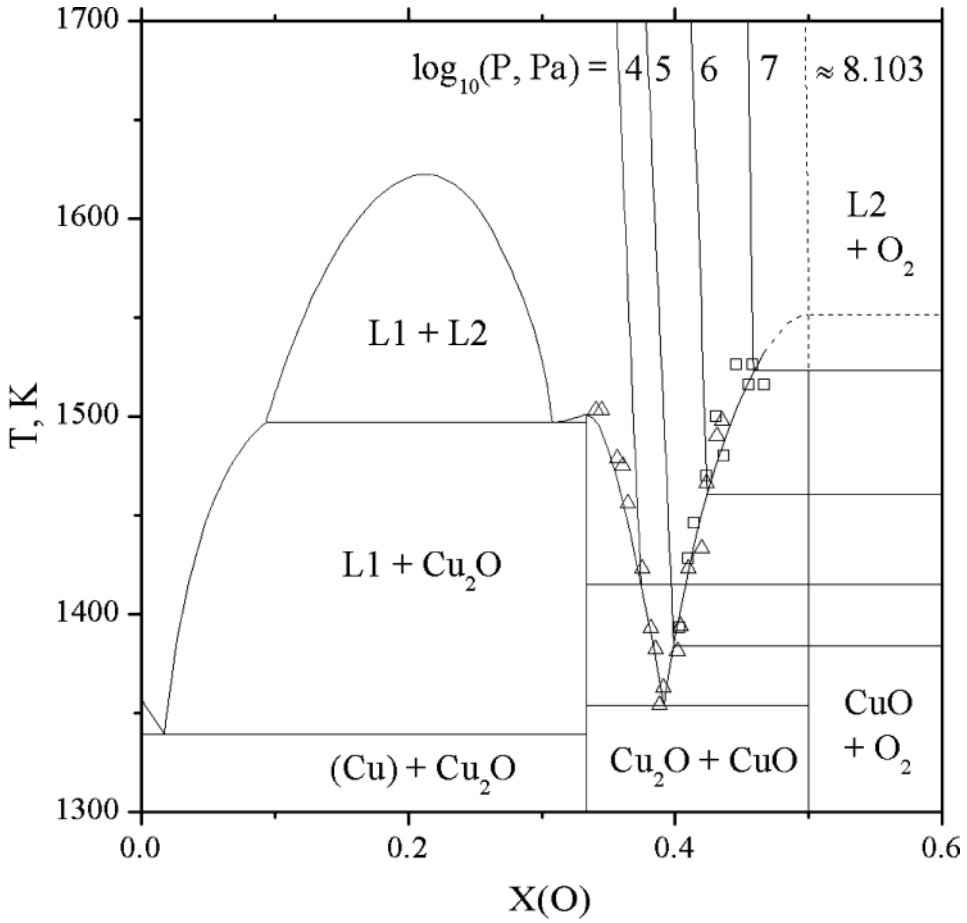

Fig. 1 Calculated Cu-O phase diagrams for different oxygen pressures: 0.01, 0.1, 1, 10, and 126.8 MPa along with the experimental results from Ref 4 (triangles) and Ref 5 (squares). The dashed part of the CuO liquidus line above the experimental information of 11 MPa is regarded as speculative.

function of a half mole gaseous O_2 at any temperature T and pressure p related to the reference pressure $p_0 = 0.1$ MPa.[23] Atomic oxygen and gaseous copper oxide have not been taken into account in this assessment.[24,25] Previous calculations showed that their fractions are very low ($<10^{-6}$ at 1600 K and 100 MPa).

2.2 Ionic-Liquid Phase

The two-sublattice model of ionic liquids was used to describe the liquid phase.[26] In this model, liquid species like Cu_2O and Cu_2O_2 can simply be translated into $(Cu^{+1})_2(O^{-2})_1$ and $(Cu^{+2})_2(O^{-2})_2$, where the parentheses define two different sublattices for cations and anions, respectively. A homogeneous concentration space is enabled by the appearance of negatively charged vacancies Va^{-q} to be located on the anion sublattice. The whole formula for the ionic liquid used in this work is given by $(Cu^{+1},Cu^{+2},Cu^{+3})_p(O^{-2},Va^{-q})_q$, where the cation sublattice carries Cu^{+1}, Cu^{+2}, as well as the higher valent Cu^{+3} ion and the anion sublattice is occupied by O^{-2} and vacancies. To obtain electroneutrality, the values of p and q are set to:

$$p = 2 \cdot y_{O^{-2}} + q \cdot y_{Va^{-q}} \quad \text{(Eq 2)}$$

$$q = 1 \cdot y_{Cu^{+1}} + 2 \cdot y_{Cu^{+2}} + 3 \cdot y_{Cu^{+3}} \quad \text{(Eq 3)}$$

Starting from pure copper, defined by $(Cu^{+1})_1(Va^{-1})_1$, the successive oxidation of copper is described by the following two reactions:

$$\tfrac{1}{2}(Cu^{+2})_2(Va^{-2})_2 + 2(Cu^{+1})_2(O^{-2})_1 \leftrightarrow 3(Cu^{+1})_1(Va^{-1})_1 + (Cu^{+2})_2(O^{-2})_2 \quad \text{(Eq 4a)}$$

with the net reaction:

$$Cu^{+1} \leftrightarrow Cu^{+2} + Va^{-1} \quad \text{(Eq 4b)}$$

and

$$\tfrac{1}{3}(Cu^{+3})_3(Va^{-3})_3 + \tfrac{3}{2}(Cu^{+2})_2(O^{-2})_2 \leftrightarrow (Cu^{+2})_2(Va^{-2})_2 + (Cu^{+3})_2(O^{-2})_3 \quad \text{(Eq 5a)}$$

with the net reaction:

$$Cu^{+2} \leftrightarrow Cu^{+3} + Va^{-1} \quad \text{(Eq 5b)}$$

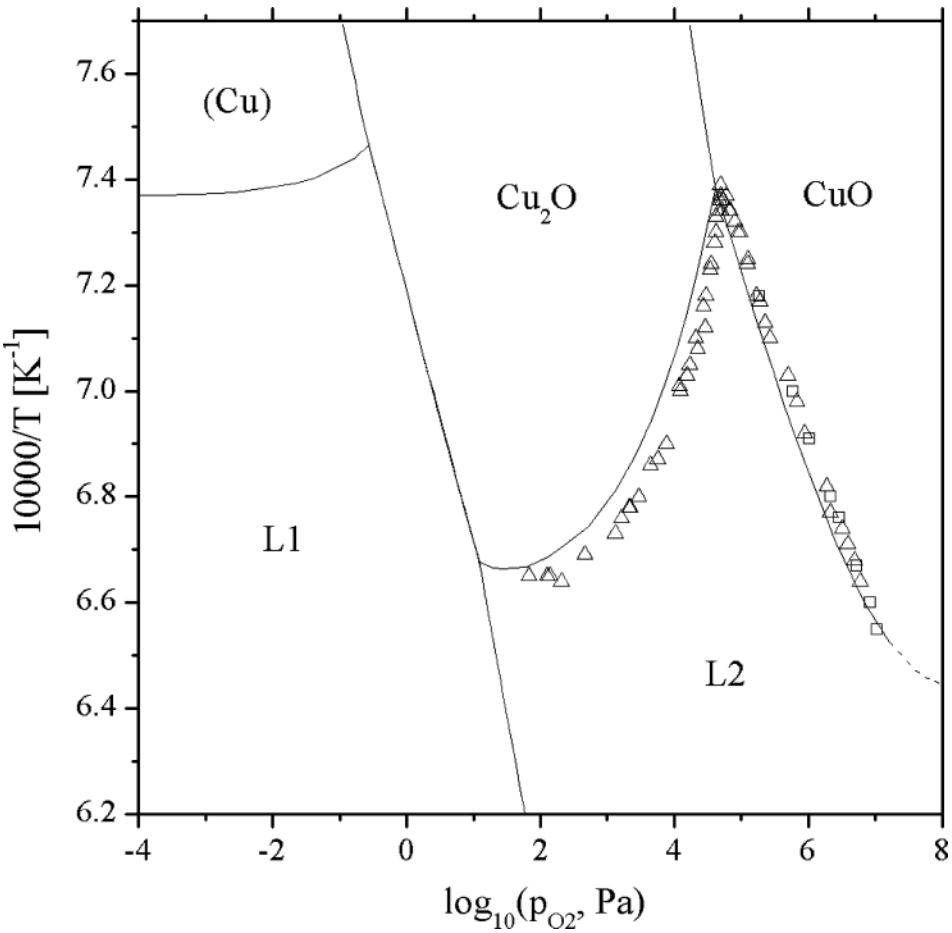

Fig. 2 Calculated Cu-O potential diagram for oxygen pressures from 10^{-2} to 10^{8} Pa including the experimental results from Ref 4 (squares) and Ref 5 (triangles). The dashed part of the CuO liquidus beyond the experimental information of 11 MPa is regarded as speculative.

The latter reaction assumes the formation of a molecular-like Cu_2O_3 species, which is expressed as $(Cu^{+3})_2(O^{-2})_3$ in the sublattice model. Considering the reactions of Eq 4a and 5a to be reversible and setting their total energy yield equal to zero, the molar Gibbs energy of $(Cu^{+1})_1(Va^{-1})_1$, $(Cu^{+2})_2(Va^{-2})_2$, and $(Cu^{+3})_3(Va^{-3})_3$ can be given by:

$$G^{liquid}_{Cu^{+1}:Va^{-1}} \equiv G^{liquid}_{Cu} \quad \text{(Eq 6)}$$

$$G^{liquid}_{Cu^{+2}:Va^{-2}} = 3 \cdot G^{liquid}_{Cu} + G^{liquid}_{Cu^{+2}:O^{-2}} - 2 \cdot G^{liquid}_{Cu^{+1}:O^{-2}} \quad \text{(Eq 7)}$$

$$\begin{aligned} G^{liquid}_{Cu^{+3}:Va^{-3}} &= 2 \cdot G^{liquid}_{Cu^{+2}:Va^{-2}} + G^{liquid}_{Cu^{+2}:O^{-2}} - \frac{3}{2} \cdot G^{liquid}_{Cu^{+2}:O^{-2}} \\ &= 6 \cdot G^{liquid}_{Cu} + \frac{1}{2} \cdot G^{liquid}_{Cu^{+2}:O^{-2}} + G^{liquid}_{Cu^{+3}:O^{-2}} \\ &\quad - 4 \cdot G^{liquid}_{Cu^{+1}:O^{-2}} \end{aligned} \quad \text{(Eq 8)}$$

In Eq 6-8, the value of G^{liquid}_{Cu} refers to the Gibbs energy of one mole liquid copper,[23] and the Gibbs energies of the species $(Cu^{+1})_2(O^{-2})_1$, $(Cu^{+2})_2(O^{-2})_2$, and $(Cu^{+3})_2(O^{-2})_3$ can be denoted by $G^{liquid}_{Cu^{+1}:O^{-2}}$, $G^{liquid}_{Cu^{+2}:O^{-2}}$, and $G^{liquid}_{Cu^{+3}:O^{-2}}$ with each referring to $p + q$ moles of ions. In the sense of the mathematical formalism of the two-sublattice model, all of the above mentioned species represent a complete set of the so called end-members, which define the whole concentration space of the phase. The total Gibbs energy of the liquid phase G_{liquid} can be expresses by its weighted sum, where y_i is the site fraction of the ionic component i (including vacancies) in either one of the two sublattices:

$$\begin{aligned} G^{liquid} &= q \cdot y_{Cu^{+1}} \cdot y_{Va^{-1}} \cdot G^{liquid}_{Cu^{+1}:Va^{-1}} \\ &\quad + q \cdot y_{Cu^{+2}} \cdot y_{Va^{-2}} \cdot G^{liquid}_{Cu^{+2}:Va^{-2}} \\ &\quad + q \cdot y_{Cu^{+3}} \cdot y_{Va^{-3}} \cdot G^{liquid}_{Cu^{+3}:Va^{-3}} + y_{Cu^{+1}} \cdot y_{O^{-2}} \cdot G^{liquid}_{Cu^{+1}:O^{-2}} \\ &\quad + y_{Cu^{+2}} \cdot y_{O^{-2}} \cdot G^{liquid}_{Cu^{+2}:O^{-2}} + y_{Cu^{+3}} \cdot y_{O^{-2}} \cdot G^{liquid}_{Cu^{+3}:O^{-2}} \\ &\quad + \Delta S^{liquid}_{MIX} + \Delta G^{liquid}_{MIX} \end{aligned} \quad \text{(Eq 9)}$$

with

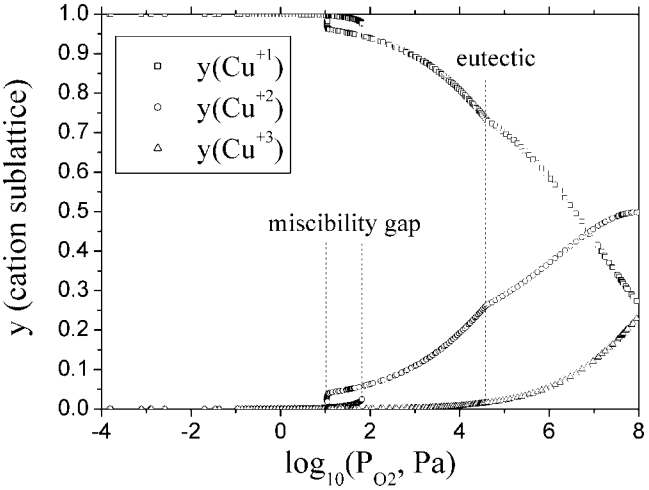

Fig. 3 Site fraction of the cation sublattice versus oxygen pressure of the homogeneous ionic liquid calculated along the liquidus lines and the boundary of the (L ↔ L1 + L2) miscibility gap, respectively. The discontinuities are related to the appearance of the miscibility gap and the (L ↔ Cu_2O + CuO) eutectic.

$$\Delta S_{MIX}^{liquid} = p \cdot R \cdot T \cdot [y_{Cu^{+1}} \cdot \ln(y_{Cu^{+1}}) + y_{Cu^{+2}} \cdot \ln(y_{Cu^{+2}}) + y_{Cu^{+3}} \cdot \ln(y_{Cu^{+3}})] + q \cdot R \cdot T \cdot [y_{O^{-2}} \cdot \ln(y_{O^{-2}}) + y_{Va^{-q}} \cdot \ln(y_{Va^{-q}})] \quad \text{(Eq 10)}$$

and

$$\Delta G_{MIX}^{liquid} = y_{Cu^{+1}} \cdot y_{O^{-2}} \cdot y_{Va^{-q}} \cdot L^{liquid,0}_{Cu^{+1}:O^{-2},Va^{-q}} + y_{Cu^{+1}} \cdot y_{O^{-2}} \cdot y_{Va^{-q}} \cdot L^{liquid,1}_{Cu^{+1}:O^{-2},Va^{-q}} \cdot (y_{O^{-2}} - y_{Va^{-q}}) + y_{Cu^{+1}} \cdot y_{O^{-2}} \cdot y_{Va^{-q}} \cdot L^{liquid,2}_{Cu^{+1}:O^{-2},Va^{-q}} \cdot (y_{O^{-2}} - y_{Va^{-q}})^2 + y_{Cu^{+1}} \cdot y_{Cu^{+2}} \cdot y_{O^{-2}} \cdot L^{liquid,0}_{Cu^{+1},Cu^{+2}:O^{-2}} \quad \text{(Eq 11)}$$

In Eq 9 and 10, the expression ΔS_{MIX}^{liquid} is the ideal entropy term of the mixed ionic components and ΔG_{MIX}^{liquid} of Eq 9 and 11 is the excess Gibbs energy considering their interaction energies. If the only binary interactions are examined, the parameters $L_{i:j,k}^{liquid,n}$ of Eq 11 refer to the excess Gibbs energy of the interaction between the ionic components j and k (including vacancies) located in one sublattice, where the other sublattice is filled by species i (A comma separates species on the same sublattice, and a colon separates species on the two different sublattices. The number n behind the phase designation is the number of the term in Redlich-Kister polynomial).

2.3 Solid Solution Phases

The solubility of oxygen in solid Cu [face-centered cubic (fcc) structure] is very low and is considered as a simple real solution of copper and oxygen (approx. 0.02 at.% O at ~1340 K); i.e., no special crystallographic characteristic is assumed. Therefore, according to Hallstedt et al.,[3] the fcc phase is modeled by the substitutional solution model.[27] Its molar Gibbs energy is:

$$G_m^{fcc} = x_{Cu} \cdot G_{Cu}^{0,fcc} + x_O \cdot G_O^{0,fcc} + R \cdot T \cdot [x_{Cu} \cdot \ln(x_{Cu}) + x_O \cdot \ln(x_O)] + x_{Cu} \cdot x_O \cdot L_{Cu,O}^{fcc,0} \quad \text{(Eq 12)}$$

where x_i is the mole fraction of element i. The Gibbs energy of pure copper has been published by Dinsdale,[23] and the Gibbs energy of fcc-oxygen $G_O^{0,fcc}$ as well as the interaction parameter $L_{Cu,O}^{fcc,0}$ are taken from Hallstedt et al.[3] As an alternative to the substitutional solution model of Hallstedt et al.,[3] Hallstedt and Gauckler modeled the Gibbs energy of the fcc phase by an interstitial solution model with one interstitial site per Cu atom. This assumption was made in analogy to other fcc metals, where light elements occupy octahedral interstices. However, in the case of the Cu–O system, there is still no experimental evidence for interstitial oxygen. Besides that, the difference in calculated oxygen solubility from the two models is minimal.

2.4 Stoichiometric Oxides

The two oxides CuO and Cu_2O show no deviations from stoichiometry.[28,29] Their thermodynamic properties can by expressed by:

$$G^{Cu_nO} = a + b \cdot T + c \cdot T \cdot \ln(T) + d \cdot T^2 + e \cdot T^{-1} \quad \text{(Eq 13)}$$

where $n = 1$ in case of CuO and $n = 2$ in case of Cu_2O. The parameters a through e are constant values, which have been determined[3] for the Cu_2O compound. The paramagnetic-antiferromagnetic transition[30,31] in CuO with a Néel temperature at 230 K is far below the modeled temperature range, and was not considered in this work.

3. Optimization of Parameters

Optimization of model parameters was carried out using the computer program PARROT included in the Thermo-Calc databank system.[32] The program minimizes the sum of squared errors by adjusting the relative weight of each experiment. The optimization is repeated until a satisfactory description of the experimental data points is reached. The phase diagram information in the present optimization comprises data on the Cu_2O and CuO liquidus lines at pressures between 1.27×10^{-4} and 10.73 MPa.[4,5] It could be shown (Fig. 3), that the occurrence of the Cu^{+3} species in the liquid phase does not affect the low-pressure description ($p \leq 1.3 \times 10^{-4}$ MPa) of the system given by Hallstedt and coworkers[3,9] Therefore, the optimization was limited to the parameter describing the formation of the species $(Cu^{+3})_3(Va^{-3})_3$ and $(Cu^{+3})_2(O^{-2})_3$ as well as the parameters for the CuO compound. In the final optimization these parameters were refined simultaneously. The results of optimization are given in Table 1, which also presents all further parameters used in this assessment. In Table 1 each function for Gibbs energy of the individual phases refers to the standard reference state enthalpy (HSER) of pure elements at $p_0 = 1$ bar, $T = 298.15$ K and a standard structure listed under general references.

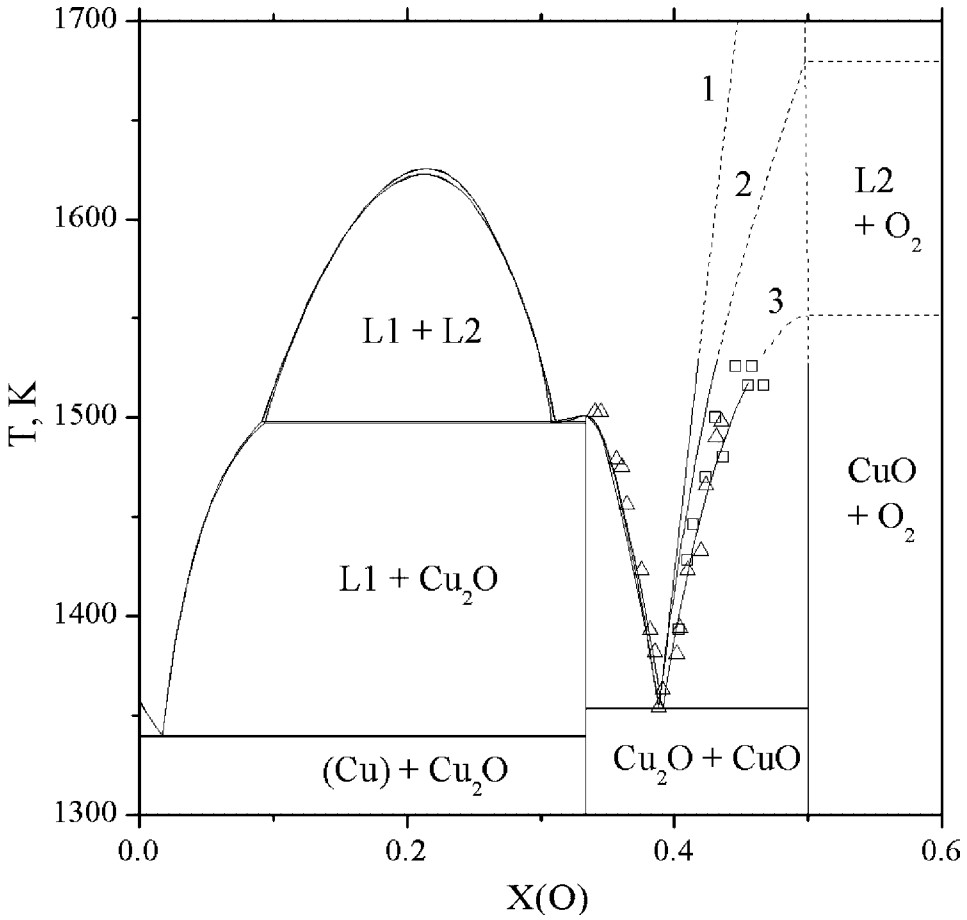

Fig. 4 Calculated Cu-O phase diagrams: (1) Hallstedt (Ref 3), (2) Hallstedt (Ref 9), (3) this work in comparison with the experimental results from Roberts and Smyth (Ref 4, triangles) and Kosenko and Emel'chenko (Ref 5, squares). The part of the CuO liquidus above the experimental limit of 11 MPa is regarded as speculative.

4. Results and Discussion

Calculated *x-T* phase diagrams for different oxygen pressures of 0.01, 0.1, 1, 10, and 126.8 MPa as well as the potential diagram together with the experimental information are presented in Fig. 1 and 2. The optimization of parameters yield the best fit to the experimental liquidus data of Roberts and Smyth[4] and Kosenko and Emel'chenko[5] and the Gibbs energy of the CuO phase[11,12] between 298 and 1364 K.

With extrapolation of the Gibbs energy function of gaseous O_2 to pressures higher than 11 MPa, the congruent melting point for the CuO compound was calculated to be at 1551 K and 126.8 MPa. Under these conditions the ionic liquid phase consists approximately of $y_{Cu^{+1}} = y_{Cu^{+3}} = 0.25$, $y_{Cu^{+2}} = 0.50$, $y_{O^{-2}} \approx 1$ and $y_{Va} < 10^{-6}$ on the two different sublattices. For standard pressure of 0.1 MPa the Cu^{+3}-content on the cation sublattice drops to a small value of $y_{Cu^{+3}} = 0.02$ ($y_{Va} \approx 1.5 \times 10^{-3}$). The pressure dependence of the site fractions of the cation sublattice is shown as calculated in Fig. 3. The strong reduction of the Cu^{+3}-content with falling oxygen pressure verifies the preliminary assumption of the complied independence between low-pressure and high-pressure description of the system.

The new assessed coordinate of the O-rich eutectic is slightly moved to an oxygen concentration of $X_O = 0.392$ at a temperature of 1354 K. This is consistent with the previous calculations of Hallstedt and Gauckler[9] ($X_O \approx 0.388$ at 1353 K) and the experimentally determined eutectic[4] shown in Fig. 1.

The fitted parameters of the CuO phase are valid from 298 K up the experimental high pressure melting point at 1526 K and 10.73 MPa. Between 298 and 1364 K the calculated Gibbs energy of CuO is in good agreement with experimental data published in Ref 11 and 12.

Figure 4 shows a comparison between the present Cu-O phase diagram and two previously diagrams calculated by Hallstedt and coworkers.[3,9] The present analysis provides a considerably improved fit to the experimental data points of the pressure dependant CuO liquidus line compared with previous attempts. One important consequence is the dramatic reduction of the extrapolated temperature and pressure for congruent melting of the CuO compound (1551 K and 126.8 MPa in this work compared with 1916 K and ~10^7 MPa in Hallstedt et al.[3] and 1675 K and ~10^6 MPa in Hallstedt and Gauckler).[9] Moreover, the composition difference between liquidus line and the stoichiometric concentration CuO is more reduced with increasing pressure

Table 1 Thermodynamic parameters of the Cu-O system

Parameter	Equation (J)	$[T_{min} \le T < T_{max}]$
GENERAL REFERENCE STATE		
element: Cu structure: fcc-A1		…
element: 0 structure: 1/2 mol O2(GAS)		…
COMPONENTS OF THE SYSTEM		
Va		…
O_2		…
Cu^{+1}		…
Cu^{+2}		…
Cu^{+3}		…
O^{-2}		…
GAS		
$G^0_{1/2O_2}$ – HSER(O)(c)	= GHSEROO	[298.15 ≤ T < 6000 k]
IONIC-LIQUID		
$G^{liquid}_{Cu^{+1}:Va^{-1}}$ – HSER(Cu)(a)	= GCULIQ	[298.15 ≤ T < 3200 K]
$G^{liquid}_{Cu^{+2}:Va^{-2}}$ – HSER(Cu)(a)	= 3 × GCULIQ + GCUCUOO – 2 × GCUCUO	…
$G^{liquid}_{Cu^{+3}:Va^{-3}}$ – HSER(Cu)	= 6 × GCULIQ + 0.5 × GCUCUOO + GCUCUOOO – 4 × GCUCUO	…
$G^{liquid}_{Cu^{+1}:O^{-2}}$ – 2 × HSER(Cu) – HSER(O)(a)	= GCUCUO	…
$G^{liquid}_{Cu^{+2}:O^{-2}}$ – 2 × HSER(Cu) – 2 × HSER(O)(a)	= GCUCUOO	…
$G^{liquid}_{Cu^{+3}:O^{-2}}$ – 2 × HSER(Cu) – 3 × HSER(O)	= GCUCUOOO	…
$L^{liquid,0}_{Cu^{+1}:O^{-2},Va^{-q}}$(a)	= 13,287 + 11.82 × T	…
$L^{liquid,1}_{Cu^{+1}:O^{-2},Va^{-q}}$(a)	= –17,125 + 11.52 × T	…
$L^{liquid,2}_{Cu^{+1}:O^{-2},Va^{-q}}$(a)	= 21,762 – 10.15 × T	…
$L^{liquid,0}_{Cu^{+1},Cu^{+2}:O^{-2}}$(a)	= –106,048 + 70 × T	…
fcc		
G^{fcc}_{Cu} – HSER(Cu)(b)	= GHSERCU	[298.15 ≤ T < 3200 K]
G^{fcc}_{O} – HSER(O)(b)	= 1,000,000 + GHSEROO	[298.15 ≤ T < 6000 K]
$L^{fcc,0}_{Cu,O}$(b)	= –1,017,730 + 29.6 × T	…
Cu_2O		
G^{Cu_2O} – 2 × HSER(Cu) – HSER(O)(b)	= –193,230 + 360.057 × T – 66.26 × T × ln(T) – 0.00796 × T^2 + 374,000 × T^{-1}	…
CuO		
G^{CuO} – HSER(Cu) – HSER(O)	= –178,002.39 + 275.159239 × T – 44.965711 × T × ln(T) – 0.010809208 × T^2 + 1,369,987.3 × T^{-1}	…
FUNCTIONS		
GHSERCU(c)	= –7770.458 + 130.485235 × T – 24.112392 × T × ln(T) – 0.00265684 × T^2 + 1.29223 × 10^{-7} × T^3 + 52,478 × T^{-1}	[298.15 ≤ T < 1358 K]
	–13,542.026 + 183.803828 × T – 31.38 × T × ln(T) + 3.64167 × 10^{29} × T^{-9}	[1358 ≤ T < 3200 K]
GHSEROO(c)	= –3480.87 – 25.503038 × T – 11.1355 × T × ln(T) – 0.005098875 × T^2 + 6.61845833 × 10^{-7} × T^3 – 38,365 × T^{-1}	[298.15 ≤ T < 1000 K]
	–6568.763 + 12.659879 × T – 16.8138 × T × ln(T) – 5.957975 × 10^{-4} × T^2 + 6.781 × 10^{-9} × T^3 + 262,905 × T^{-1}	[1000 ≤ T < 3300 K]
	–13,986.728 + 31.259624 × T – 18.9536 × T × ln(T) – 4.25243 × 10^{-4} × T^2 + 1.0721 × 10^{-8} × T^3 + 4,383,200 × T^{-1}	[3300 ≤ T < 6000 K]
GCULIQ(c)	= 12,964.735 – 9.511904 × T + GHSERCU – 5.8489 × 10^{-21} × T^7	[298.15 ≤ T ≤ 1358 K]
	–46.545 + 173.881484 × T – 31.38 × T × ln(T)	[1358 ≤ T < 3200 K]
GCUCUO(a)	= –114,945 + 307.98 × T – 67.71 × T × ln(T)	…
GCUCUOO(a)	= 1.333333 × GCUCUO + 16,236 – 20 × T	…
GCUCUOOO	= 1.666667 × GCUCUO – 33,972.668 + 25.917348 × T	…

(a) Parameter is taken from Ref 9
(b) Parameter is taken from Ref 3
(c) Parameter is taken from Ref 23

than suggested by previous models. These two facts imply important consequences for the preparation of CuO from the melt, where CuO crystal growth under elevated pressure is facilitated. In particular, the reduced composition difference at the moving melt-crystal interface for high pressures enables higher growth velocities and improves the crystal perfection.[18] It is expected that the similar tendencies hold for more complex cuprates, too.

5. Summary

Parts of the equilibrium phase diagram of the Cu-O system were reassessed using the calculation of phase diagrams technique CALPHAD based upon experimental information on phase equilibria up to oxygen pressures of 11 MPa. Compared with previous models a considerable modification of the CuO liquidus line as function of oxygen pressure was inferred. With the presence of Cu^{+3} ions in the liquid phase, of our thermodynamic model was a new approach. The present results provide an excellent fit to the experimental data. The extrapolated congruent melting point of the CuO compound at a temperature of 1551 K and a pressure of 126.8 MPa suggests an opportunity of direct solidification of CuO at high pressure. Thus, the importance of reasonable thermodynamic modeling of the Cu-O system for melting and crystal growth experiments at elevated pressure is obvious.

References

1. R.J. Cava, B. Batlogg, R.B. Vandover, J.J. Krajewski, J.V. Waszcak, R.M. Fleming, W.F. Peck, L.W. Rupp, P. Marsh, A.C.W.P. James, and L.F. Schneemeyer, Superconductivity at 60-K in LA2-XSRXCACU2O6—The Simplest Double-Layer Cuprate, *Nature,* 1990, Vol 345 (No. 6276), p 602-604
2. E. Dagotto and T.M. Rice, Surprises on the Way from One- to Two-Dimensional Quantum Magnets: The Ladder Materials, *Science,* 1996, Vol 271 (No. 5249), p 618-623
3. B. Hallstedt, D. Risold, and L. J. Gauckler, Thermodynamic Assessment of the Copper-Oxigen System, *J. Phase Equilibria,* Vol 15, 1994, p 483-499
4. H.S. Roberts and F.H. Smyth, The System Copper: Cupric Oxide: Oxygen, *J. Am. Chem. Soc.,* Vol 43, 1921, p 1061-1079
5. A.V. Kosenko and G.A. Emel'chenko, Equilibrium Phase Relationships in the System Cu-O under High Oxygen Pressure, *J. Phase Equilibria,* Vol 22, 2001, p 12-19
6. R. Schmid, A Thermodynamic Analysis of the Cu-O System with an Associated Solution Model, *Metall. Trans. B,* Vol 14, 1983, p 473-481
7. A. Boudéne, K. Hack, A. Mohammad, D. Neuschütz, and E. Zimmermann, Experimental Investigating and Thermochemical Assessment of the System Cu-O, *Z. Metallkd,* Vol 83, 1992, p 663-668
8. V.A. Lysenko, *Neorganitcheskie Materialy,* Vol 34, 1998, p 1108-1114 (in Russian)
9. B. Hallstedt and L.J. Gauckler, Revision of the Thermodynamic Descriptions of the Cu-O, Ag-O, Ag-Cu-O, Bi-Sr-O, Bi-Ca-O, Bi-Cu-O, Sr-Cu-O, Ca-Cu-O and Sr-Ca-Cu-O Systems, *Computer Coupling of Phase Diagrams and Thermochemistry,* Vol 27, 2003, p 177-191
10. M.T. Calavaguera-Mora, J.T. Touron, J. Rodriquez-Viejo, and N. Clavaguera, Thermodynamic Description of the Cu-O System, *J. Alloys Compd.,* Vol 377, 2004, p 8-16
11. Termicheskie Konstanty Veshchestv, Part I: O, H, Halogenes, Inert Gases,1965; Part II: Chalcogenides,1966; Part III: N, P, As, Sb, Bi, 1969; Part IV: C, Si, Ge, Sn, Pb, 1970; Part V: B, Al, Ga, Ir, Tl, 1971; Part VI: Zn, Cd, Hg, Cu, Ag, Au, Fe, Co, Ni, Ru, Rh, Pd, Os, Ir, Pt, 1972; Part VIII: SC, Y, Lanthanides, Actinides, 1978; Part X: Alkaline Metals, 1981; P. Glushko and V.A. Medvedev, Ed., Akademyia Nauk, Moscow, U.S.S.R.
12. D.R. Stuell et al., JANAF, Thermochemical Tables, M.W. Chase, et al., Ed., U.S. Dept. of Commerce/Natl. Bur. Stand., US Governmt. Printing Office, 1971, *J. Phys. Chem. Ref. Data,* 1985, Vol 14, p 1
13. M. O'Keeffe and J-O. Brown, The Crystal Structure of Paramelanokite, Cu_4O_3, *Am. Mineral.*, Vol 63, 1978, p 180
14. Gmelin's Handbuch der Anorganischen Chemie, Kupfer-Teil, B-Lieferung 1, (Gremlin's Handbook of Anorganic Chemistry) Verlag Chemie, Weinheim, Germany, 1958, p 133-138 (in German)
15. R. Scholder and U. Voelskow, Über Cuprate (III), (About Cuprates [III]) *Z. Anorg. Allg. Chem.,* Vol 256, 1951, p 266 (in German)
16. G. Krabbes, W. Bieger, U. Wiesner, and A. Teresiak: Isothermal Sections and primary Crystallization in the Quasiternary $YO_{1.5}$-BaO-CuO_x System at $p(O_2) = 0.21\ 10^5$ Pa, *J. Solid State Chem.,* 1993, *103*, p 420-432
17. U. Ammerahl, G. Dhalenne, A. Revcolevschi, J. Berthon, and H. Moudden: Crystal growth and Characterization of the Spin-Ladder Compound $(Sr,Ca)_{14}Cu_{24}O_{41}$, *J. Cryst. Growth,* 1998, 193, p 55-60
18. G. Behr, W. Löser, M-O. Apostu, W. Gruner, M. Hücker, L. Schramm, D. Souptel, and J. Werner: Floating Zone Growth of CuO Under Elevated Oxygen Pressure and its Relevance for the Crystal Growth of Cuprates, *J. Cryst. Growth,* Vol 40 (No.1/2), 2005, p 21-25
19. J.B. Goodenough and A. Manthiram, Crystal Chemistry and Superconductivity in the Copper Oxides, *Chemistry of High Temperature Superconductors,* C.N.R. Rao, Ed., World Scientific Publishing Co., 1991, p 1-56
20. D.D. Sarma, Investigation of the Electronic Structure of the Cuprate Superconductors Using High-Energy Spectroscopies, Chemistry of High Temperature Superconductors, C.N.R. Rao, Ed., World Scientific Publishing Co. Pte. Ltd., 1991, p 348-378
21. D.D. Sarma, O. Strebel, C.T. Simmons, U. Neukirch, and G. Kaindl, Electronic Structure of High-T_c Superconductors from Soft-X-ray Absorption, *Phys. Rev. B,* Vol 37, No. 16, 1988, p 9784-9787
22. *CRC Handbook of Chemistry and Physics,* D.R. Lide, Ed., CRC Press, 1994, p 6-49
23. A. Dinsdale, SGTE Data for Pure Elements, *CALPHAD*, Vol 15, 1991, p 317-425
24. R.H. Lamoreaux and D.L. Hildenbrand, High-Temperature Vaporization Behaviour of Oxides II. Oxides of Be, Mg, Ca, Sr, Ba, B, Al, Ga, In, Tl, Si, Ge, Sn, Pb, Zn, Cd, and Hg, *J. Phys. Chem. Ref. Data,* Vol 16, 1987, p 419-443
25. O. Knacke, O. Kubaschewski, and K. Hesselmann, *Thermochemical Properties of Inorganic Substances 1,* Springer-Verlag, 1991, p 603

26. B. Sundman, Modification of the Two-Sublattice Model for Liquids, *CALPHAD*, Vol 15, No. 2, 1991, p 109-119
27. N. Saunders and A.P. Miodownik, *CALPHAD, Calculation of Phase Diagrams, A Comprehensive Guide,* Pergamon Materials Series Vol.1, Elsevier Science Ltd, 1998, p 92
28. J. Xue and R. Dieckmann, The Non-Stoichiometry and the Point Defect Structure of Cuprous Oxide ($Cu_{2-\delta}O$), *J. Phys. Chem. Solids,* Vol 51, 1990, p 1263-1275
29. J. Xue and R. Dieckmann, The High-Temperature Phase Diagram of the Cu-O System in Stability Region of Cuprous Oxide ($Cu_{2-\delta}O$), *High Temp. High Press.,* Vol 24, 1992, p 271-284
30. M.M. O'Keeffe and F.S. Stone, The Magnetic Susceptibility of Cupric Oxide, *J. Phys. Chem. Solids,* Vol 23, 1962, p 261-266
31. M.S. Seehra, Z. Feng, and R. Gopalakrishnan, Magnetic Phase Transitions in Cupric Oxide, *J. Phys. C, Solid State Phys.,* Vol 21, 1988, p L1051-L1054
32. B. Jansson, Trita-Mac-0234, Royal Institute of Technology, Stockholm, Sweden,1984